Structure and Properties of Cyano-Substituted Poly(2,5-dialkoxy-*p*-phenylene vinylene)s

Show-An Chen* and En-Chung Chang

Chemical Engineering Department, National Tsing-Hua University, Hsinchu, Taiwan 30043, China

Received October 14, 1997; Revised Manuscript Received March 18, 1998

ABSTRACT: Soluble, crystallizable cyano-substituted poly(2,5-dialkoxy-*p*-phenylene vinylene)s (RO-CNPPV)s having the alkoxy groups hexyloxy, octyloxy, and decyloxy were synthesized by use of the Knoevenagel-type condensation method and characterized by use of X-ray diffraction, differential scanning calorimetry, and UV−vis and photoluminescence (PL) spectroscopy measurements. In the ordered phase, the polymers have a two-layer structure with side chain aligned in the all-trans conformation lying on the same plane of the coplanar main chains. However, the presence of the bulky cyano group on the vinylene segment leads to a deviation from coplanarity and poor stacking of the main chains and therefore the absence of vibronic transitions in the UV−vis and PL spectra (which usually appear in the PPV and RO-PPVs). In addition, as temperature increases, the extent of aromatic ring distortion increases gradually, causing a continuous increase in the *d*-spacing between two neighboring stacking subchains (d_m), which increases up to 16% at the end of melting, but the side chain retains the same orientation and the *d*-spacing between two successive layers (d_s) expands by only about 3%. This is opposite to that of poly(3-dodecylthiophene) having a vibronic transition, for which d_m remains constant and d_s increases by 22% mainly in the melting region. In the melting range, although the aromatic rings distort to a higher extent, and in the meantime the side chains become more coil-like and randomly oriented, both can recover to their original alignments after cooling down to below the melting region. In the entire thermal process, a significant thermochromism occurs with the optical absorption maximum shifting by 81 nm compared to that of poly(3-dodecylthiophene), 100 nm, while the emission maximum blue-shifts by 94 nm. As temperature rises well above T_m (by more than 40 °C), the aromatic rings distort to a high extent such that the side chains intermingle with each other, causing a strongly hindered relaxational motion of the main chains after the cooling. They can recover to their original state only by redissolving and then recasting. No liquid crystalline state in the RO-CNPPVs is observed.

Introduction

Poly(phenylene vinylene)s (PPVs) are one of the important series of conjugated polymer for their environmental stability and outstanding photo- and electroluminescent properties. Since the Cambridge group[1] found that PPV in the neutral state can be used as a light-emitting layer for light-emitting diodes in 1990, electro-optical properties of PPV and its derivatives have been extensively studied. Since PPV is insoluble, in order to improve its processability, flexible side chains, such as alkoxy,[2,3] have been introduced on the aromatic rings of the main chain. In addition to processability improvement, color-tuning is also desirable, which can be achieved efficiently by controlling the conjugation length of the main chain to provide polymers emitting light from blue to orange yellow,[2−5] by introducing electron-withdrawing groups such as halogen,[6−9] nitro,[10,11] and cyano[12,13] and electron-donation groups such as an alkoxy group[2−4] on the aromatic ring to give a blue-shift and red-shift, respectively, or by introducing an electron-withdrawing group such as cyano[14,15] on the vinylene segment to give polymers (CNPPV) emitting visible light at longer wavelength, that is, red.

Reports on the structure characterizations of PPV and its derivatives are reviewed below. For PPV, its unit cell in the crystalline state was found to be monoclinic[16,17] with the dihedral angle (the angle between the plane of the phenyl ring and that of the vinylene segment) 8°, 9°, and 13° at 20, 200, and 400 °C, respectively, on the basis of XRD data. After doping with $FeCl_3$, the unit cell changed from monoclinic to orthorhombic.[18] For alkoxy-substituted PPV (RO-PPV), when the length of the OR group is short, that is, diethoxy,[19] the side chains do not align regularly; when it is long, that is, 2-(dodecyloxy)-5-methoxy,[20] the side chains are considered to align in the trans-conformation to form a layered structure as those of the rigid rod polymers: poly(3-alkylthiophene)s (P3ATs),[21,22] poly(2,5-dialkoxy-*p*-phenylene)s (PPPs),[23] *N*-alkylated polyanilines (*N*-PANs),[24] polyesters[25−27] and polyamides,[27] and poly(2,5-dialkoxy-*p*-phenylene ethynylene)s (PPEs),[28,29] in which the side chain can align in various fashions, such as extended two-layer structure, tilting, and interdigitation. When one of the hydrogen atoms on the vinylene segment is replaced by the bulky cyano group (which induces steric hindrance), the polymer is found to still retain its coplanar conformation with inter-ring torsion angles of $0 \pm 15°$ due to solid-state packing effects as in the case of PPV and its derivatives.[30] However, fully coplanar conformations are considered to be highly unlikely.[31] In viewing the literature above, no report on thermal transitions of PPVs and cyano-substituted PPVs as well as accompanying conformation changes is given.

This work reports the structure characterization of soluble cyano-substituted poly(2,5-dialkoxy-*p*-phenylene vinylene) (RO-CNPPV) based on the measurements using X-ray diffraction, differential scanning calorimetry, and ultraviolet−visible spectroscopy, in order to understand alignment and packing of the main chains and side chains across the glass and melting transitions.

* To whom correspondence should be addressed. E-mail: sachen@che.nthu.edu.tw.

S0024-9297(97)01507-6 CCC: $15.00
Published on Web 07/03/1998

Scheme 1

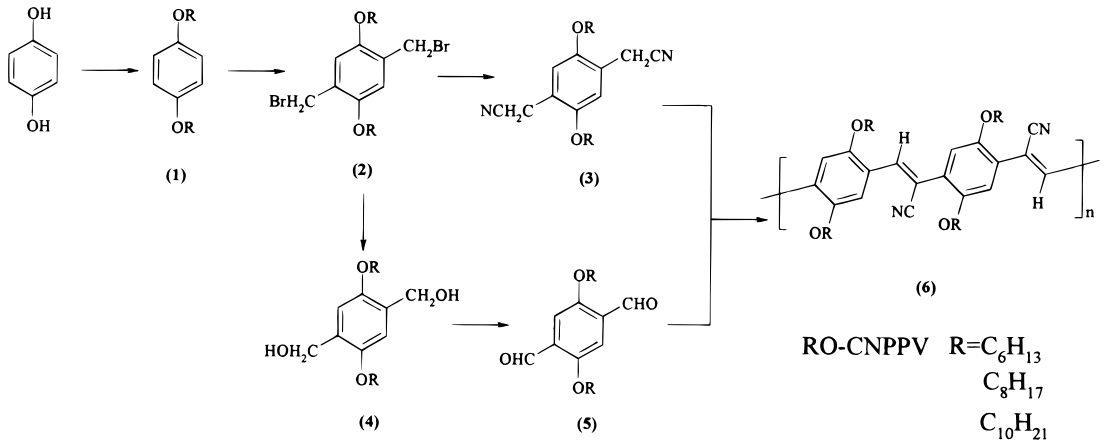

The alkoxy-substitutents investigated involve OC_6H_{13} (C_6O), OC_8H_{17} (C_8O), and $OC_{10}H_{21}$ ($C_{10}O$).

Experimental Section

Synthesis. The syntheses of the three RO-CNPPVs and their intermediates are mainly in accordance with the methods proposed in the literature.[14,15,32−35] The reaction procedures described in the Appendix are for the preparation of cyano-substituted poly(2,5-dihexyloxy-*p*-phenylene vinylene) (C_6O-CNPPV) and are also applicable for the other two RO-CNPPVs with the alkoxy groups C_8O (C_8O-CNPPV) and $C_{10}O$ ($C_{10}O$-CNPPV). The polymerization step is a Knoevenagel-type condensation, as proposed by Holmes and co-workers.[14,15] All the reaction steps are described in Scheme 1.

Instrumentation. Infrared spectra (IR) were recorded using a Perkin-Elmer model 983 infrared spectrometer. Ultraviolet−visible spectra (UV−vis) of RO-CNPPV at −100 to 250 °C were recorded using a UV−vis−NIR spectrometer (Perkin-Elmer UV−vis−NIR spectrometer, Lambda 19). The spectrometer was equipped with a variable temperature cell to allow spectra to be measured under vacuum from −100 to 250 °C; the soaking time was 10 min at each specific temperature, and the heating rate used was about 5 °C/min during heating. The testing sample was prepared by casting RO-CNPPV solution in chloroform on a piece of quartz. ^{1}H NMR spectra were recorded at 300 MHz with a Varian Gemini 300 MHz spectrometer.

Gel permeation chromatography with an UV detector at 500 nm and three columns in series (American GPC Linear 15 mm from American standards polymer corporation) was used to measure molecular weight distributions (MWDs) relative to polystyrene standards at room temperature. The calibration curve was determined by use of six MW standards from 2200 to 7.5×10^5. The carrier solvent used was degassed THF at the flow rate 1 mL/min.

X-ray diffractions (XRDs) were measured using a Siemens D5000 diffractometer from 25 to 210 °C. The X-ray beam was nickel-filtered Cu Kα (=1.54 Å) radiation from a sealed tube operated at 30 kV and 20 mA. The testing sample was prepared by coating on a platinum plate from the polymer solution (about 50 mg/mL) in chloroform and drying under ambient conditions and was then mounted in the sample cell. The thickness of the coated films was about 0.05−0.1 mm. For the annealing study, a sample of similar thickness was coated on a glass plate; after drying, it was annealed at 100 °C under vacuum for 24 h and then subjected to the XRD measurement at 25 °C. The temperature of the measurement was controlled by resistor heating. Diffraction intensity data were obtained from 2 to 35° (2θ) at a scan rate of 0.02 deg/s. Each scan at a specific temperature required about 30 min.

A thermogravimetric analyzer (DuPont Model TGA 2950) was used to measure the weight loss of polymer films during the temperature scan from 25 to 600 °C with the heating rate 10 °C/min in a stream of nitrogen. A differential scanning calorimeter (DuPont Model DSC 2910 Modulated DSC) was used to examine thermograms in the temperature range −100 to 250 °C with the heating rate 5 °C/min (sinusoidal ripple heating rate modulated with a period of 60 s and an amplitude of 2 °C) in a stream of nitrogen. The advantages of modulated DSC over conventional DSC are that it can separate the overlapping of reversing and nonreversing thermal transitions, as well as relaxation phenomena from the glass transition. Other advantages include better precision, resolution, and sensitivity. The optical texture was observed on a Leitz polarized optical microscope with a THMS600 heating stage at the heating rate 20 °C/min.

Table 1. Average Molecular Weights of RO-CNPPVs Relative to Polystyrene Standards

polymer	$10^{-4}\bar{M}_n$	$10^{-4}\bar{M}_w$	PD[a]
C_6O-CNPPV	1.8	4.5	2.5
C_8O-CNPPV	1.4	3.0	2.2
$C_{10}O$-CNPPV	1.9	4.2	2.2

[a] PD: $\bar{M}_w/\bar{M}_n$.

Results and Discussion

Gel Permeation Chromatography (GPC). All the three RO-CNPPVs can be dissolved in common organic solvents, such as $CHCl_3$, THF and toluene. The number- and weight-average molecular weights ($\bar{M}_n$ and $\bar{M}_w$) and polydispersity index (PD) (relative to the molecular weight standards of polystyrene) are listed in Table 1. The $\bar{M}_w$'s are on the order of 10^4, which is sufficiently high to be considered as a high polymer.

X-ray Diffraction (XRD). X-ray diffraction (XRD) patterns of the as-casted films of RO-CNPPVs at room temperature are shown in Figure 1; their characteristic angles at intensity maxima and corresponding values of *d*-spacing calculated using Bragg's law are listed in Table 2. Each RO-CNPPV exhibits a strong diffraction peak at low diffraction angle (2θ = 2.85−4.21°) and, except for C_6O-CNPPV, two weak diffraction peaks at 5.5−7.0° and 8.5−11°, which decrease with increasing length of side chain, and a broad scattering peak ranging from 2θ = 15 to 25° centered at about 20° is observed (the inset of Figure 1), which is independent of the length of side chains. After annealing at 100 °C for 24 h under vacuum, the intensities of diffraction peaks at the low and wide angles of the as-casted films become sharper, but the locations of these peaks have no appreciable change, indicating an increase in crystallinity. Because of the similarity in the XRD patterns, only that of $C_{10}O$-CNPPV is shown in Figure 3.

Since only one peak is observed at the wide angle, about 20°, for the samples with and without the an-

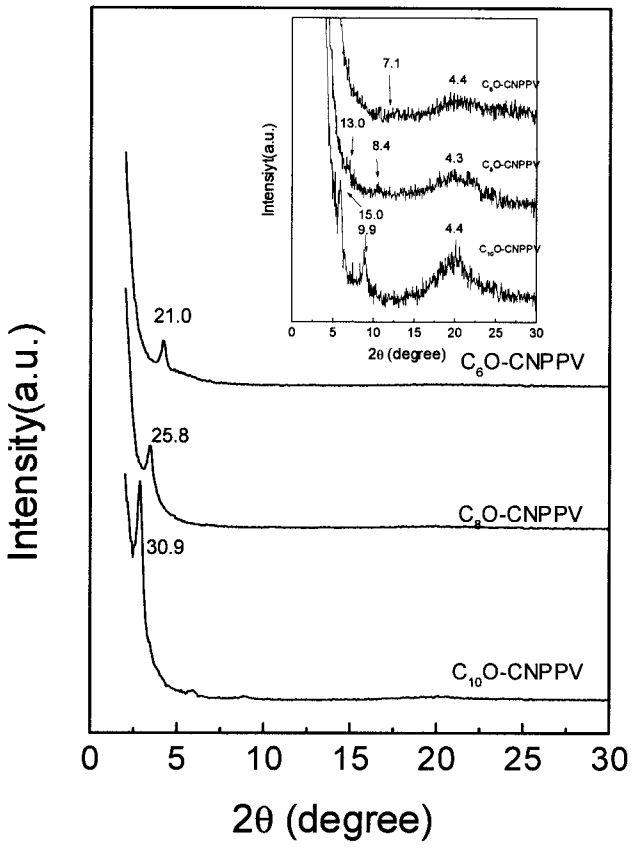

Figure 1. X-ray diffraction patterns of RO-CNPPVs at 25 °C. The peaks are labeled with *d*-spacings in angstroms.

nealing, the diffractions due to intermolecular stacking of the ordered main chains and due to random arrangement of the amorphous chains must overlap. This indicates that the stacking of the main chains in the ordered phase is poor. This situation is different from that of the other rigid rod polymers, such as P3ATs,[21,22] PPPs,[23] N-PANs,[24] PPEs,[28,29] polyesters,[25−27] and polyamides,[27] in which the diffraction peak attributed to the intermolecular stacking (in addition to the broad amorphous peak) appears for the as-casted sample and becomes sharper after annealing. PPV has been found to have a diffraction peak at the wide angle $2\theta = 20.9°$, which was attributed to the intermolecular stacking of the main chains.[17] Similarly, each RO-CNPPV also has a diffraction peak (at about 20°) very close to that for PPV, which can thus be attributed also to the intermolecular stacking of coplanar subchains (or intraplanar spacing). The corresponding *d*-spacing of RO-CNPPV (about $d = 4.4$ Å) is slightly larger than that of PPV ($d = 4.24$ Å). This is due to the introduction of a cyano group on the vinylene segment, which can lead to a slight distortion of the planar main chain, as was found for the cyano-substituted oligo(*p*-phenylene vinylene),[36] in which a dihedral angle of 10.1° between the cyano group and the benzene ring exists in its unit cell.

For the strong diffraction peaks at the low diffraction angles (4.21°, 3.42°, and 2.85°) of C_6O-, C_8O and $C_{10}O$-CNPPV, their corresponding values of *d*-spacing are 20.99, 25.81, and 30.93 Å, respectively, indicating that the *d*-spacing increases with the length of side chain. Since this peak does not appear for PPV, it must relate to an ordered alignment of the side chains as in the cases of P3ATs,[21,22] PPPs,[23] N-PANs,[24] PPEs,[28,29] polyesters,[25−27] and polyamides.[27] The space between two neighboring coplanar subchains on the same plane must be filled with side chains.

The values of the *d*-spacing of the diffraction peaks at low (d_s) and wide (d_m) angles versus the number of carbon atoms of the side chains of RO-CNPPVs give two straight lines, as shown in Figure 2. The latter is independent of side chain length, and the former is identical to the calculated value for each RO-CNPPV based on two layer packing with two neighboring side chains (all-trans conformation) on the same side-chain axis of two neighboring subchains laying on the same plane (see Figure 9a). The calculated value of d_s is obtained by summing the diameter of a benzene ring, 2.8 Å (estimated from the geometric structure of benzene), and twice the sum of $(m + 1)$ times the C−C bond length projected on the axis of the extended side chain (1.25 Å) and the terminal C−H bond projected on the same axis (0.6 Å). Here *m* is the number of carbon atoms in the alkoxy group, and the ether group is counted as a methylene unit. The slope of this line is 1.25 Å per methylene group, matching with an all-trans conformation of the C atoms in the side chains. Thus, it can be inferred that the side chains of RO-CNPPV align in the all-trans conformation along the direction perpendicular to the chain axis and lie on the same plane of the coplanar subchains.

In order to investigate effects of temperature variation on the structure of RO-CNPPVs, XRD patterns for the three RO-CNPPVs at various temperatures from 25 to 210 °C were measured and their corresponding values of d_s and d_m were calculated as listed in Table 2. Because of the similarity in the XRD patterns, only those of $C_{10}O$-CNPPV are shown in Figure 3a. For $C_{10}O$-CNPPV, as temperature increases from 25 to 140 °C, the diffraction peak at low angle shifts slightly from 3.0° to 2.9° ($d_s = 30.0$ to 30.9 Å), and the diffraction intensity increases; it then disappears at 210 °C. The same trend is also observed for higher order diffractions at about 5.5−7° and 8−13°. As temperature drops to room temperature, this peak appears again and its intensity is higher than that before the heating scan. This means that the spacing between the two successive layers d_s expands slightly with temperature by about 3% before melting, while the increase in peak intensity during the heating to 140 °C and after the cooling is due to the annealing effect, allowing more side chains to align in an ordered fashion. Figure 3b shows the amplified patterns such that the diffraction patterns at wide angles can be visualized clearly, which shows that the diffraction peak shifts from about 20° ($d_m = 4.4$ Å) at 25 °C to the lower angle 17.5° ($d_m = 5.1$ Å) at 210 °C. The increased molecular thermal motion causes an increase in d_m (intraplanar spacing) by 16%. The complete disappearance of the diffraction peaks at low angle and the broadening of the peak at wide angle at 210 °C indicate that $C_{10}O$-CNPPV has a crystalline melting transition before 210 °C, during which the ordered subchains and side chains melt simultaneously. When the upper limit is increased to 300 °C, the XRD pattern after cooling down to room temperature exhibits no diffraction peak at low angle and a featureless broad peak at the wide angle. It indicates that the crystallinity of the polymer after the heat treatment becomes so low and is undetectable by XRD. Similar thermal behaviors are also observed for the other two RO-CNPPVs (see Table 2). These results are consistent with their corresponding DSC thermograms and UV−

Table 2. X-ray Diffraction Maxima and Their Corresponding *d*-Spacings of RO-CNPPVs

temp (°C)	2θ (deg)/d-spacing (Å)					
	C_6O-CNPPV		C_8O-CNPPV		$C_{10}O$-CNPPV	
25	4.4/20.0	20.4/4.4	3.5/25.4	20.6/4.3	3.0/30.0	20.0/4.4
80	4.3/20.4	20.2/4.4	3.5/25.4	19.2/4.6	2.9/30.4	19.4/4.6
140	4.2/20.9	19.4/4.6	3.4/25.9	19.0/4.7	2.9/30.9	18.2/4.9
210	4.2/20.8	18.2/4.9		18.2/4.9		17.5/5.1
R25[a]	4.2/21.0	20.2/4.4	3.4/25.8	20.0/4.4	2.9/30.9	20.0/4.4
A25[b]	4.5/19.6	21.3/4.2	3.7/23.9	20.5/4.3	3.1/28.5	20.3/4.4
calcd values[c] of d-spacing (Å)	21.5		26.5		31.5	

[a] Returned to room temperature by cooling from 210 °C. [b] Measured at 25 °C after the sample was annealed at 100 °C under vacuum for 24 h. [c] Calculated from the ideal all-trans model.

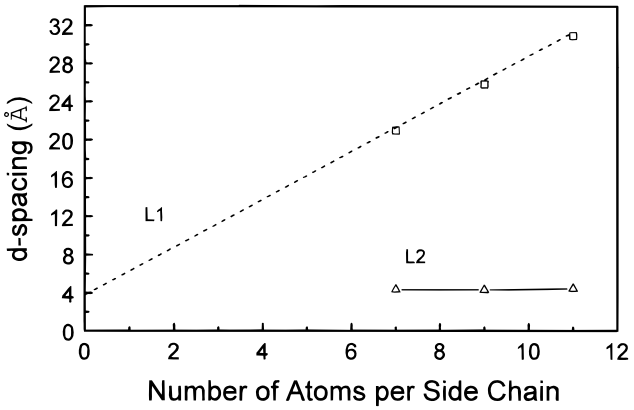

Figure 2. Correlation of layer periodicity as obtained from XRD data and the number of carbon atoms per side group for RO-CNPPVs. The oxygen is counted as a methylene group: (- - -) theoretical; (□) d_s-spacing; (△) d_m-spacing.

vis spectra at various temperatures, as will be discussed in the next two sections.

Differential Scanning Calorimetry (DSC). DSC thermograms of the first heating/cooling and second heating scans of RO-CNPPVs from −100 to 250 °C are shown in Figure 4, and their characteristic values are listed in Table 3. In the heating scan, C_6O-, C_8O-, and $C_{10}O$-CNPPV exhibit obvious endothermic peaks at 210, 204, and 183 °C, respectively. These characteristic temperatures can be assigned to the melting temperature (T_m), since a homogeneous and featureless morphology and no liquid crystalline texture are observed at these temperatures by use of polarized optical microscopy and, in addition, flowing fluid is observed visually at 200 °C for $C_{10}O$-CNPPV. The weak melting peak of C_8O-CNPPV is probably due to the low MW and/or a presence of saturated linkages resulting from the Michael addition in the polymerization step. The decrease of T_m with increasing side chain length can be attributed to the higher free volume (and therefore lower thermal energy for molecular motion) provided by the longer flexible side chains. No side chain melting is observed, quite different from the case of P3AT, for which a side chain melting transition was observed when the carbon number of the side chain was 10 or more.[21,37−39] In the cooling scan, however, no exothermic peak for each RO-CNPPV is observed, indicating that no crystallization occurs. This is not due to thermal degradation, since no change in their IR spectra and no weight loss below 300 °C are observed, but is due to the fact that the loss of crystallinity after the heating scan to 250 °C does not recover after the cooling scan even after storage at room temperature for 3 days as examined by DSC. The absence of thermal degradation can be further supported by the fact that, as $C_{10}O$-CNPPV is heated to 250 °C for about 30 min and then cooled down to room temperature, it can be redissolved completely in chloroform and the recast solid sample has T_m = 182 °C and ΔH_m = 15.1 J/g (Figure 5 and Table 3); both values are very close to those of the original sample (183 °C and 16.7 J/g).

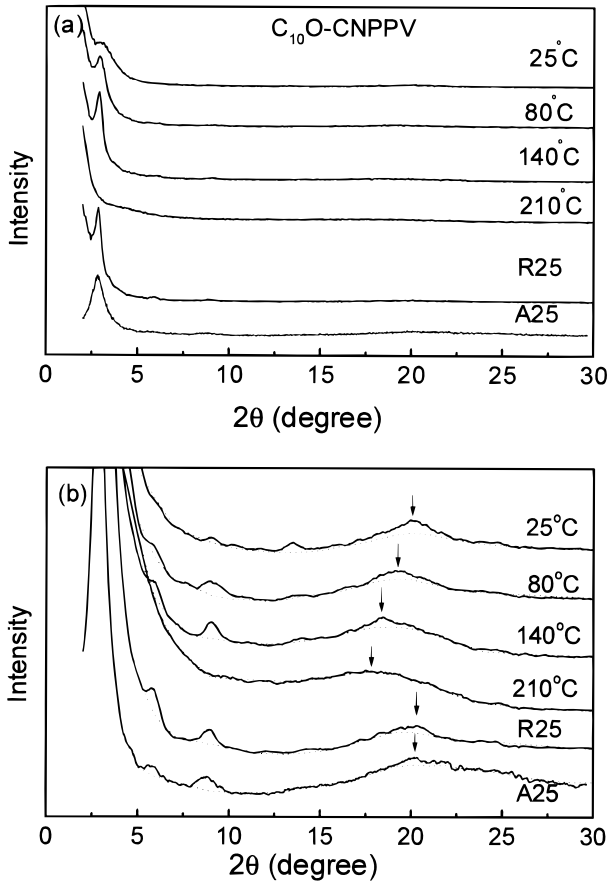

Figure 3. X-ray diffraction patterns of $C_{10}O$-CNPPV at various temperatures: (a) the entire patterns; (b) amplified patterns for increasing the visibility of the portions with 2θ above 5°. R25 means "after cooling from 210 to 25 °C"; A25 means "measured at 25 °C after annealing at 100 °C for 24 h under vacuum".

As the upper temperature limit of the first heating scan drops by 40 °C (from 250 to 210 °C) for $C_{10}O$-CNPPV, in the cooling scan, an exothermic peak due to crystallization in the range 150−185 °C (centered at 172 °C) is observed (Figure 5). The second heating scan shows a T_m at 180 °C, lower than that of the first heat scan by only 3 °C. A similar result is also observed for C_6O-CNPPV as the upper temperature limit of the first scan is set at the temperature 20 °C above its T_m.

In addition to the melting transition, a step drop in the heat flow curves can also be observed in both

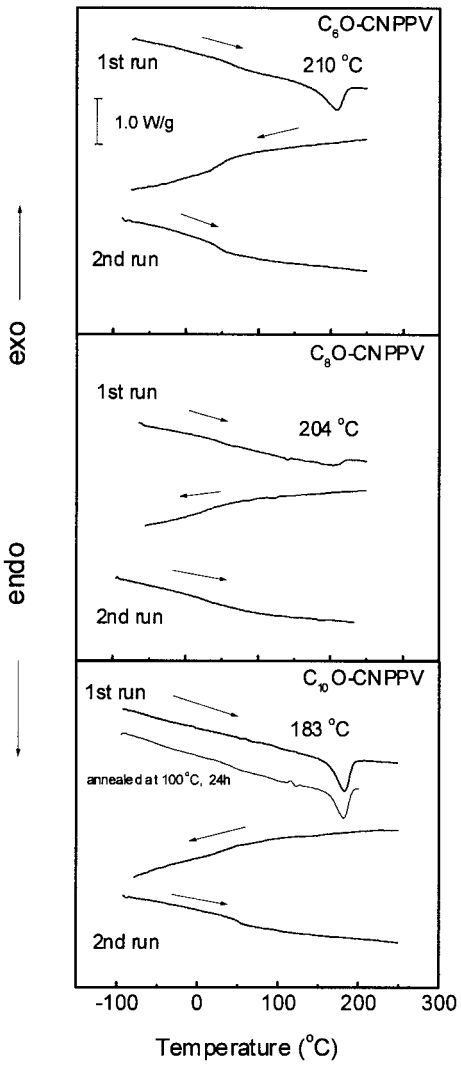

Figure 4. DSC thermograms of RO-CNPPVs with the scan range from −100 to 250 °C.

Table 3. Characteristic Temperature Range (°C) of Various Transitions Determined from DSC and UV−vis

	DSC (°C)[a]			ΔH_m	tran-	UV−vis (°C)	
polymer	onset	peak[c]	end	(J/g)	sition[b]	onset	end
C_6O-CNPPV	170	210	225	15.0	T_m	175	250
	20	45	70		T_g	50	120
	133	184	200	7.6	T_c		
C_8O-CNPPV	160	204	225	9.6	T_m	150	225
	10	35	70		T_g	10	75
	n.o.[d]	n.o.	n.o.	n.o.	T_c		
C_{10}O-CNPPV	155	183	200	16.7	T_m	125	200
	160[e]	183	200	17.2			
	10	41	65		T_g	0	50
	150	172	187	9.5	T_c		

[a] Scan range: from −100 to 250 °C. [b] T_m is determined from the heating process; T_g and T_c are determined from the cooling process. Both T_m and T_g are taken from Figure 4, and T_c is taken from Figure 5. [c] T_g is determined from the peak of the first-order derivative of the cooling curve in Figure 4. [d] n.o. means "not observed". [e] After annealing at 100 °C for 24 h under vacuum.

heating and cooling scans, which can be assigned to the occurrence of a glass transition. The drops in the cooling scan and second heating (Figure 4) are obvious if the upper temperature limit of the first scan is 250 °C, since the crystallinity in the sample decreases dramatically after the first heating scan. The center of the transition range is taken as the glass transition

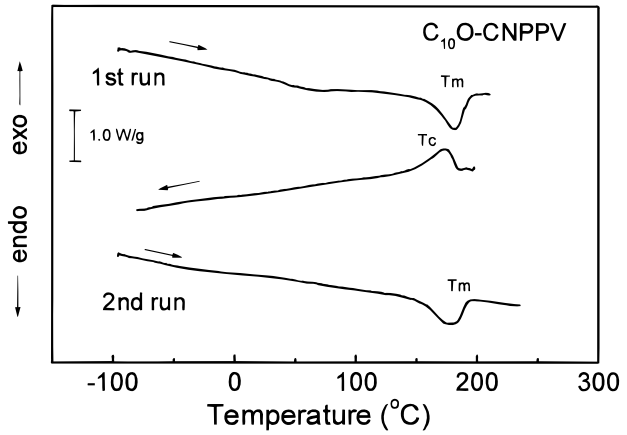

Figure 5. DSC thermograms of C_{10}O-CNPPV with the scan range from −100 to 210 °C.

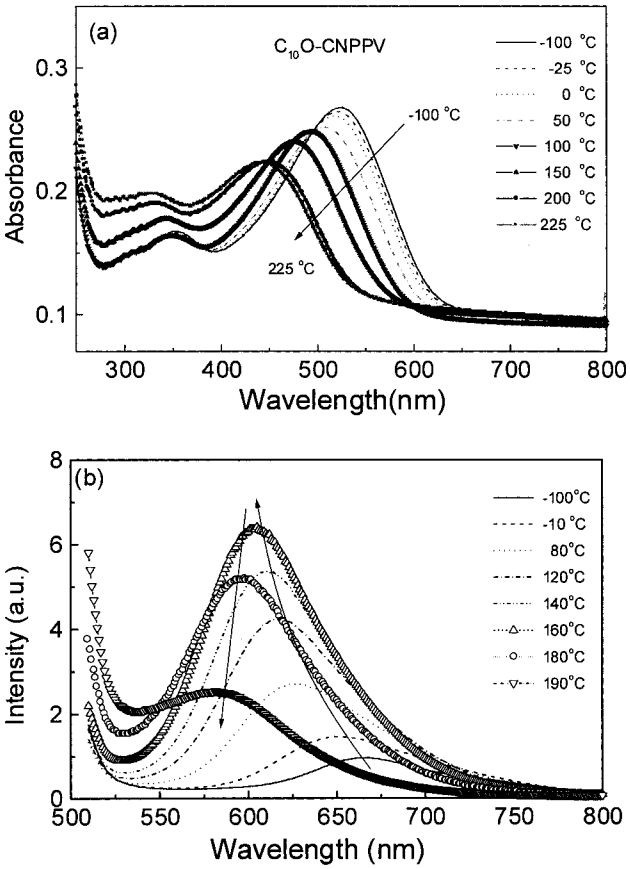

Figure 6. (a) UV−vis absorption and (b) PL spectra of C_{10}O-CNPPV solid films at various temperatures.

temperature (T_g), as listed in Table 3.

Ultraviolet−Visible (UV−vis) and Photoluminescent (PL) Spectroscopies. UV−vis and PL spectra of RO-CNPPVs from −100 to 250 °C were recorded, and only those of C_{10}O-CNPPV are presented in Figure 6 because of their similarity. As can be seen, in the visible range 400−700 nm, only single absorption and emission peaks appear, indicating that no vibronic transition occurs in the RO-CNPPVs. The vibronic transition has been found to exist in PPV and its derivatives with alkoxy substitutents on the aromatic rings[40] and the other conjugated polymers such as P3ATs[41] and PPEs[28] and appears as multiabsorption and -emission peaks. The absence of a vibronic transition would indicate an existence of significant ring

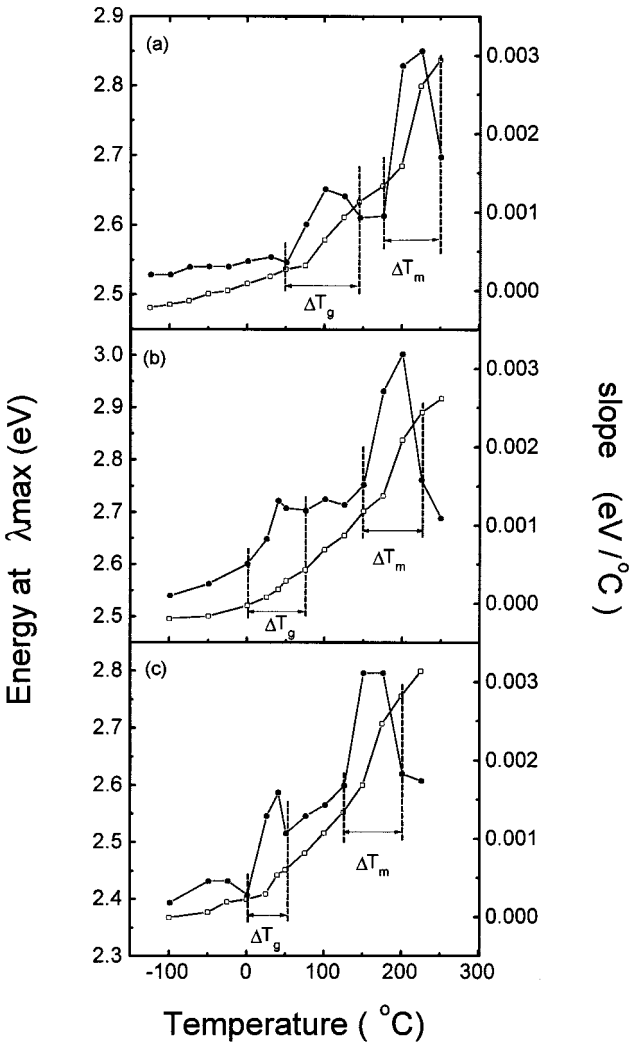

Figure 7. Plots of the energy of the absorption maximum (□) and the differential value (●) in the UV−vis spectra versus temperature for thin films of RO-CNPPVs: (a) C_6O-CNPPV; (b) C_8O-CNPPV; (c) C_{10}O-CNPPV.

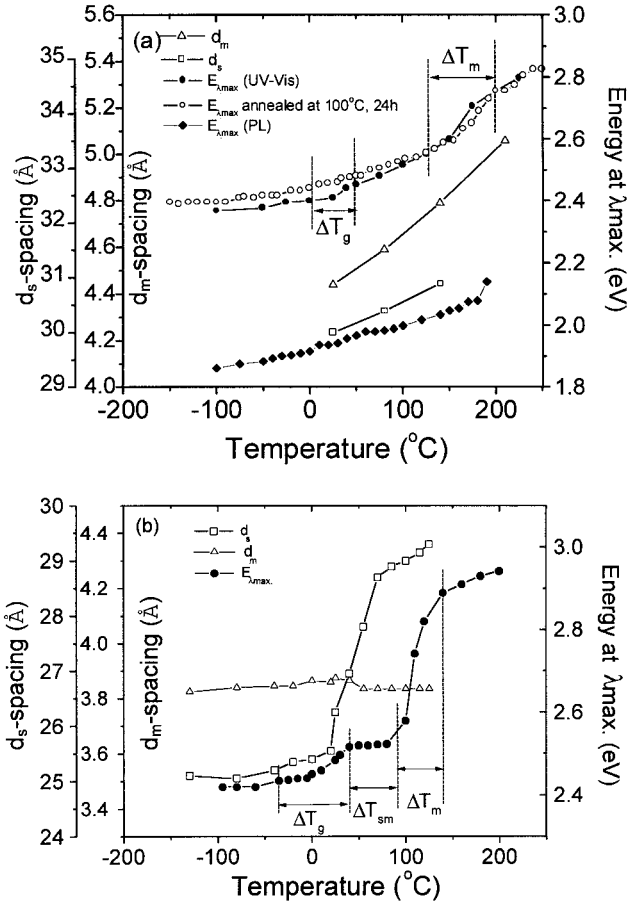

Figure 8. Variations of the *d*-spacing (d_s and d_m) and the energy at λ_{max} ($E_{\lambda_{max}}$) with temperature of (a) C_{10}O-CNPPV and (b) P3DDT. The data for $E_{\lambda_{max}}$ and cell parameters for P3DDT were taken from refs 21 and 22, respectively. ΔT_g, ΔT_{sm}, and ΔT_m are the transition temperature ranges of glassy to rubbery states, side chain melting, and main chain melting, respectively.

distortion in the main chains even at low temperature, which probably originates from the addition of the bulky cyano group on the vinylene segment.

As can be seen from Figure 6a, when temperature varies across both glass and melt transitions, the absorption λ_{max} of C_{10}O-CNPPV shifts by 81 nm from 525 nm at −100 °C to 444 nm at 225 °C, which is much larger than those of PPV and RO-PPV, about 25 nm from −100 to 240 °C and is comparable to that of poly(3-dodecylthiophene) (P3DDT),[21] about 100 nm from −100 to 190 °C. This would indicate the occurrence of a significant thermochromic effect. The color of the film changes from deep red in the lower temperature range (below 100 °C) to orange-red at 150 °C to orange-yellow at 250 °C, and it returns to the original color as the film cools down to room temperature. The variations in emission spectra of C_{10}O-CNPPV in this temperature range (Figure 6b) show the same trend as those of absorption spectra. The emission λ_{max} shifts by 94 nm from 668 nm at −100 °C to 574 nm at 190 °C. This blue-shift is significantly larger than those of PPV and RO-PPV,[42] about 15 nm from −100 to 240 °C.

Plots of the energy of the absorption maximum ($E_{\lambda_{max}}$) versus temperature of the three RO-CNPPVs are shown in Figure 7. Since $E_{\lambda_{max}}$ is a measurement of the energy for the $\pi-\pi^*$ transition, it is represented here in the unit of energy eV. Two transitions appear, and their temperature ranges (Table 3) are in agreement with those of the glass and melting transitions determined from DSC. The energy change across the melting transition (0.18−0.22 eV) is larger than that across the glass transition (0.05−0.1 eV), and the sum of these two energy changes (0.24−0.28 eV) is significantly lower than the energy change of the entire range from −100 °C to the end of the melting transition (200−250 °C), about 0.35−0.41 eV. This indicates that significant ring distortion, which causes a decrease in conjugation length, also occurs below and above the glass transition region. For an understanding of the conformation change in the entire thermal transition process of RO-CNPPV, d_s, d_m, and $E_{\lambda_{max}}$ of the absorption and emission spectra versus temperature of C_{10}O-CNPPV are plotted as shown in Figure 8a. As can be seen, d_m increases gradually with temperature by 16% from the onset of the glass transition to the end of the melting transition, and so do the $E_{\lambda_{max}}$ values except at the initial stage of the melting transition. But for d_s, the increase is only 3%. From these results, it can be inferred that the extent of ring distortion increases slowly with temperature starting from −100 to 0 °C, rapidly from 0 to 50 °C, covering the glass transition region and extending to the onset of the melting region, and more rapidly from 125 to 200 °C. Consequently, the spacing between two

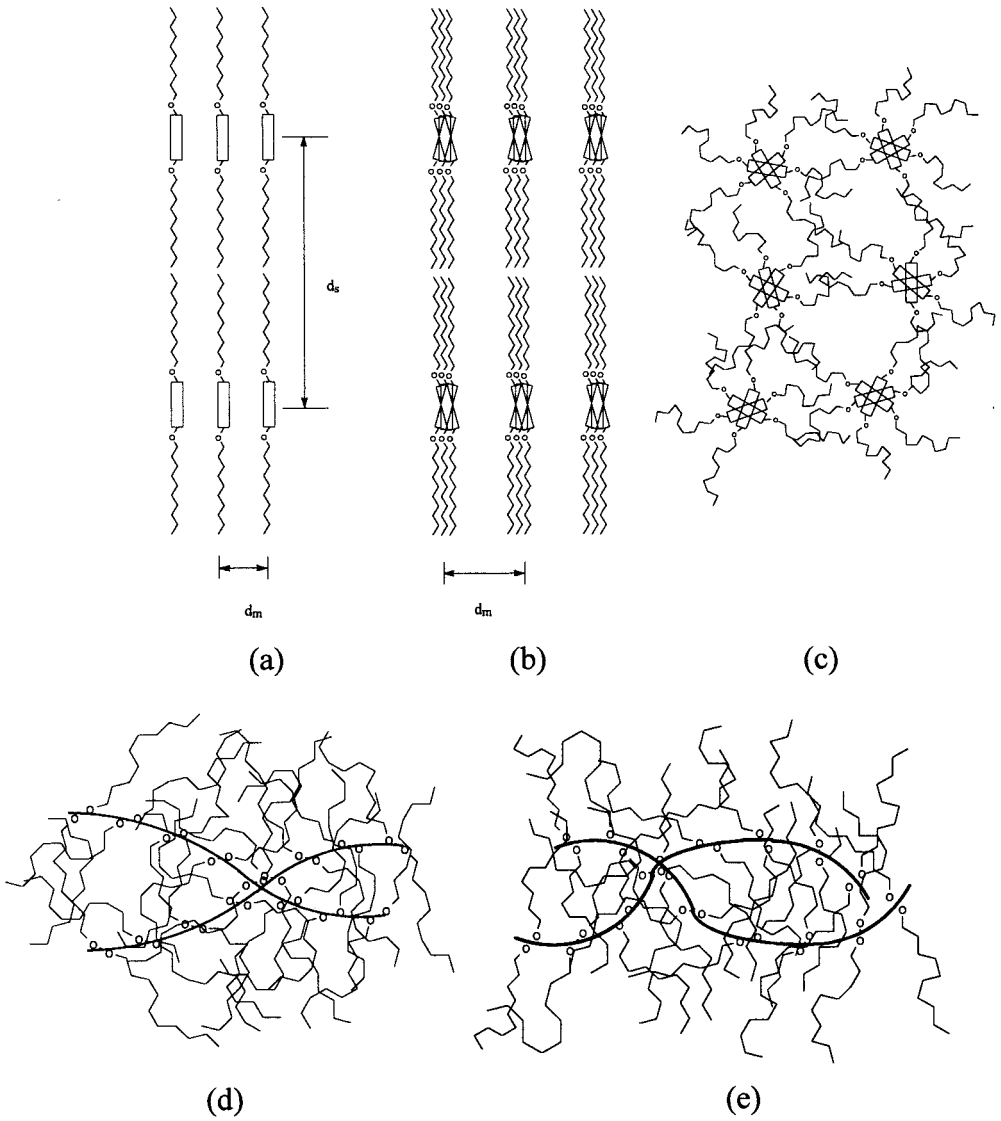

Figure 9. Schematic representation of chain alignment of RO-CNPPVs. Ordered structure (a) at low temperature (below T_g), (b) below the onset of the melting region, and (c) after (but close to) the end of the melting region. Disordered structure (d) below T_m and (e) well above T_m (The kinks represent the saturated linkages). The main chains in parts a−c are perpendicular to the plane of the paper. The heavy lines in parts d and e are the main chains.

stacking subchains d_m increases accordingly. Before the melting, the ordered side chains always retain the same direction of orientation, in spite of the continuously increased distortion of the rings in the main chain. After the melting, the extent of ring distortion is high, such that the conformation of the main chains is more or less coil-like, and the neighboring side chains could start to intermingle with each other. As the temperature is well above the end of the melting region, the aromatic rings are further distorted and the conjugational defects (saturated linkages) resulting from the Michael addition in the polymerization step could lead to the presence of kinks in the main chain. Consequently the side chains intermingle with each other to a level such that relaxational motion of the main chains is strongly hindered after cooling to a temperature below the melting region; and the degree of crystallinity of the resulting polymer is low, undetectable by DSC. Such hindered relaxational motion of the main chains does not originate from an entanglement of the main chains, since the $\bar{M}_w$ relative to that for the polystyrene standard is low, only about 4×10^4, and the actual $\bar{M}_w$ may be considerably lower. The critical MW, below which there are few or no chain entanglements, for the linear nonconjugated chain has been found to increase with the rotational barrier, from 3800 for polyethylene to 36 000 for polystyrene.[43] For conjugated polymers, the main chains are rigid and their critical MW's should be higher.

The conformation changes described above are quite different from those of the other series of soluble, crystallizable conjugated polymer, P3AT, which will be discussed below. P3DDT was found to have an orthorhombic unit cell and an alternating inverse comb[22] structure in its crystalline state, in which a reorientation of the all-trans alkyl side chain away from the direction of the coplanar main chain is considered. The cell parameter b (or $2d_m$) characterizes the d-spacing between two neighboring stacking rings and the cell parameter a (or $2d_s$) characterizes the d-spacing between two neighboring layers in which the space is filled with side chains. Measurements of the unit cell dimensions at various temperatures from −130 to 125 °C have been reported by Winokur and co-workers,[22] and those on $E_{\lambda_{max}}$ from −100 to 250 °C by one of us.[21] The results are plotted in Figure 8b. Although the variations of d_s

and $E_{\lambda_{max}}$ with temperature are similar, their transition temperatures are different; the $E_{\lambda_{max}}$ curve leads the d_s curve by about 50−60 °C. This is probably due to the sample used in the $E_{\lambda_{max}}$ measurement having an average molecular weight ($\bar{M}_w = 2.6 \times 10^5$) higher than that used in the XRD measurement (8×10^4). A lowering in $\bar{M}_w$ by 1.8×10^5 can lead to a shift in the $E_{\lambda_{max}}$ curve toward lower temperature by about 20−50 °C. Nevertheless, a comparison of these two sets of data is helpful for a determination of the variations of d_s and d_m across the two thermal transitions and, in addition, the transition of side chain melting.

In contrast to those of RO-CNPPVs, the d_m of P3DDT remains nearly constant (the deviation is only about ±1%), while its d_s increases sharply in the melting region by about 22%. With the aid of molecular dynamics in the simulation of conformation change, one of us[44] found that the sharp increase of d_s in the melting region is due to the increased tendency of the side chain to lie on the plane of the nearly coplanar main chain, though its gauche content increases, which tends to decrease d_s. The torsion angle of the main chain is about 30° and increases by about 5° across the thermal transitions. Even though the polymer experiences the transitions of side chain and main chain melting, the X-ray diffraction peaks at low and wide angles are still persistent due to its liquid crystalline characteristic at temperatures beyond the melting region.[38,45]

Structure of RO-CNPPVs and Conclusion. From the experimental results and the analysis above, the structure of RO-CNPPV is proposed as shown in Figure 9. The presence of XRD peaks at low angle and the coincidence of the d_s-spacing with twice the length of the side chain in the all-trans conformation lying on the same plane of the main chains suggest a two-layer structure for the packing of side chains, as shown in parts a and b of Figure 9. At temperatures well below T_g, the packing for main chains is nearly coplanar (part a). As temperature increases (below T_m), the extent of aromatic ring distortion also increases but the d_s-spacing remains unchanged (part b), indicating that the side chains retain the same orientation (from XRD and UV−vis). As temperature increases to the melting range, the aromatic rings distort further, and the side chains become more coil-like and randomly oriented (part c), but both can recover to their original alignments as temperature drops to below the melting region. For the disordered phase below the melting temperature of the ordered phase, the structure as in part d is suggested for the following reasons: (i) the presence of a glass transition and (ii) the existence of π-electron delocalization along the main chains before the onset of the glass transition in the disordered subchains, which is subject to an energy rise of 0.05−0.1 eV as this transition occurs. As temperature rises well above T_m, the aromatic rings are further distorted, with a presence of kinks in the main chains, causing the side chains to intermingle with each other to such an extent that relaxational motion of the main chains is strongly hindered (part e), even after the temperature drops to below the melting region. After cooling from structure e, the polymer contains only small fractions of ordered phase and its crystalline characteristics detectable from XRD and DSC are lost. At this stage, the polymer can recover to its original state only by redissolving in solvent and then casting from the solution.

The presence of the bulky cyano group on the vinylene segment leads to a deviation from coplanarity and to a poor stacking of the main chains, which cause the absence of vibronic transitions and the occurrence of significant blue-shifts by 81 and 94 nm in the absorption and emission spectra, respectively, across the entire thermal transitions. No liquid crystalline state in the RO-CNPPVs is observed.

Acknowledgment. We wish to thank the National Science Council of ROC for financial aid through the project NSC 86-2216-E-007-45.

Appendix: Preparation of Cyano-Substituted Poly(2,5-dihexyloxy-*p*-phenylene vinylene) (C_6O-CNPPV)

The chemical structures of compounds **1**−**6** are shown in Scheme 1.

Preparation of 1,4-Bis(hexyloxy)benzene (1).[32] A solution of hydroquinone (0.22 mol) and sodium methoxide (0.44 mol) in anhydrous ethanol (200 mL) was purged with nitrogen gas, stirred at room temperature, and then added dropwise to a solution of 1-bromohexane (0.45 mol) in anhydrous ethanol (50 mL). The mixture was heated to 75−80 °C with stirring to allow reaction for 24 h; then part of the solvent was removed by evaporation, and subsequently water was added. The resulting mixture was further subject to extraction with ether, drying over $MgSO_4$, and removal of the solvent. The solid so obtained was recrystallized from *n*-hexane to give colorless plates in 65% yield (mp 43 °C). ^{1}H-NMR ($CDCl_3$): δ 6.82 (s, 4H, PhH), 3.89 (t, 4H, OCH_2), 1.75 (m, 4H, CH_2), 1.6−1.2 (m, 16H, CH_2), 0.90 (t, 6H, CH_3).

Preparation of 1,4-Bis(bromomethyl)-2,5-bis-(hexyloxy)benzene (2).[33] A solution of 1,4-dihexyloxybenzene (0.05 mol) and paraformaldehyde (10 g) in 1.4-dioxane (200 mL) was purged with nitrogen gas and then added to HBr (50 mL) and acetic acid (10 mL) to allow reaction at 80 °C for 72 h, during which 5 g of paraformaldehyde and 50 mL of HBr were added at each 24 h interval. For all stages gaseous HBr was introduced by bubbling through the reaction mixture. After the reaction was completed, the precipitate was collected and then recrystallized from *n*-hexane to give compound **2** in 57% yield (mp 88 °C). ^{1}H NMR ($CDCl_3$): δ 6.85 (s, 2H, PhH), 4.53 (s, 4H, CH_2Br), 3.98 (t, 4H, OCH_2), 1.9−1.2 (m, 16H, CH_2), 0.90 (t, 6H, CH_3).

Preparation of 1,4-Bis(cyanomethyl)-2,5-bis-(hexyloxy)benzene (3).[34] To a stirred suspension of sodium cyanide in dimethyl sulfoxide (DMSO) was added compound **2** in small portions successively at 50 °C. The reaction mixture was maintained at 50 °C for an additional 1 h after the addition of compound **2** was completed and was then heated to 85 °C for 5 min. After cooling to about 40 °C, the resulting mixture was poured into 1 L of water, and the precipitate was collected and was then recrystallized from ether/chloroform to give the product in 67% yield (mp 75 °C). ^{1}H NMR ($CDCl_3$): δ 6.91 (s, 2H, PhH), 3.98 (t, 4H, OCH_2), 3.70 (s, 4H, CH_2CN), 1.9−1.2 (m, 16H, CH_2), 0.91 (t, 6H, CH_3).

Preparation of 1,4-Bis(hydroxymethyl)-2,5-bis-(hexyloxy)benzene (4).[35] A mixture of compound **3**, silver nitrate (0.103 mol), and 50% aqueous MEK (300 mL) was stirred as a suspension at room temperature in the dark for 24 h until thin layer chromatography testing on a silica gel strip (hexane/methylene chloride,

2/1 by volume) indicated the absence of the starting materials. The mixture was filtered in the dark and then washed with ether. The solid so obtained was extracted with boiling hexane/toluene (400 mL, 1/1 by volume). The extracted product in the solution was recrystallized at about 5 °C. The ether fraction was washed with water and dried over $MgSO_4$, and the solvent was removed under reduced pressure. The collected product was recrystallized from hexane/toluene (1/1 by volume) to give the diol with the total yield 33% and mp 97 °C. ^{1}H NMR ($CDCl_3$): δ 7.03 (s, 2H, PhH), 4.72 (s, 4H, CH_2O), 4.09 (t, 4H, OCH_2), 1.9−1.2 (m, 16H, CH_2), 0.91 (t, 6H, CH_3).

Preparation of 2,5-Bis(hexyloxy)terephthaldehyde (5).[35] To a cool solution (10 °C) of the diol (compound **4**) in 1,4-dioxane was added dropwise a solution of 2,3-dichloro-5,6-dicyano-1,4-benzoquinone (DDQ) in 1,4-dioxane, and then the mixture was heated to 110 °C for 48 h. After the reaction was completed, the precipitate was removed by filtration, and the solvent in the filtrate was removed by evaporation under reduced pressure using an aspirator. The crude product was purified by column chromatography on silica gel with cyclohexane/methylene chloride (4/1 by volume) as eluent. The collected product was recrystallized from *n*-hexane to give the dialdehyde product in 35% yield, mp 75 °C. ^{1}H NMR ($CDCl_3$): δ 10.52 (s, 2H, CHO), 7.43 (s, 2H, PhH), 4.09 (t, 4H, OCH_2), 1.9−1.2 (m, 16H, CH_2), 0.91 (t, 6H, CH_3).

Preparation of Polymer 6.[15] Compound **5** (1 mmol) and compound **3** (1 mmol) were dissolved in *tert*-butanol (7.5 mL) and THF (2.5 mL) at 50 °C under nitrogen purging. Potassium *tert*-butoxide (0.1 mmol) and tetra-*n*-butylammonium hydroxide (0.1 mmol, 1 M solution in methanol) were added quickly. After 20 min the mixture was poured into acidified methanol. The precipitate was collected and redissolved in chloroform and then reprecipitated in methanol to give the purified C_6O-CNPPV. ^{1}H NMR ($CDCl_3$): δ 8.10 (s, 2H, CH), 7.93 (s, 2H, CH), 7.16 (s, 2H, CH), 4.09 (m, 8H, OCH_2), 2.0−1.2 (m, 32H, CH_2), 0.90 (m, 12H, CH_3). Anal. Calcd for $(C_{42}H_{58}N_2O_4)_n$: C, 77.06; H, 8.87; N, 4.28; O, 9.79. Found: C, 76.88; H, 8.89; N, 4.28; O, 9.95. IR (KBr): 2925, 2852, 2209, 1678, 1608, 1501, 1466, 1421, 1391, 1218, 1041, 865, 722 cm^{-1}.

References and Notes

(1) Burroughes, J. H.; Bradley, D. D. C.; Brown, A. R.; Marks, R. N.; Mackay, K.; Friend, R. H.; Burns, P. L.; Holmes, A. B. *Nature* **1990**, *347*, 539.
(2) Doi, S.; Kuwabara, M.; Noguchi, T.; Ohnishi, T. *Synth. Met.* **1993**, *55*−*57*, 4174.
(3) Brown, A. R.; Greenham, N. C.; Burroughes, J. H.; Bradley, D. D. C.; Friend, R. H.; Burn, P. L.; Kraft, A.; Holmes, A. B. *Chem. Phys. Lett.* **1992**, *200*, 46.
(4) Burn, P. L.; Kraft, A.; Baigent, D. R.; Bradley, D. D. C.; Brown, A. R.; Friend, R. H.; Gymer, R. W.; Holmes, A. B.; Jackson, R. W. *J. Am. Chem. Soc.* **1993**, *115*, 10117.
(5) Yang, Z.; Sokolik, I.; Karasz, F. E. *Macromolecules* **1993**, *26*, 1188.
(6) Jin, J. I.; Park, C. K.; Shim, H. K. *Macromolecules* **1992**, *25*, 5519.
(7) Murase, I.; Ohnishi, T.; Noguchi, T.; Hirooka, M. *Synth. Met.* **1987**, *17*, 639.
(8) McCoy, R. K.; Karasz, F. E.; Sarker, A.; Lahti, P. M. *Chem. Mater.* **1991**, *3*, 941.
(9) Gregorius, R. M.; Lahti, P. M.; Karasz, F. E. *Macromolecules* **1992**, *25*, 6664.
(10) Jin, J. I.; Yu, S. H.; Shim, H. K. *J. Polym. Sci., Part B: Polym. Phys.* **1993**, *31*, 87.
(11) Jin, J. I.; Lee, Y. H.; Shim, H. K. *Macromolecules* **1993**, *26*, 1805.
(12) Shim, H. K.; Hwang, D. H.; Lee, K. S. *Makromol. Chem.* **1993**, *194*, 1115.
(13) Kim, J. J.; Kang, S. W.; Hwang, D. H.; Shim, H. K. *Synth. Met.* **1993**, *55-57*, 4024.
(14) Greenham, N. C.; Moratti, S. C.; Bradley, D. D. C.; Friend, R. H.; Holmes, A. B. *Nature* **1993**, *365*, 628.
(15) Moratti, S. C.; Cervini, R.; Holmes, A. B.; Baigent, D. R.; Friend, R. H.; Greenham, N. C.; Grüner, J.; Hamer, P. J. *Synth. Met.* **1995**, *71*, 2117.
(16) Granier, T.; Thomas, E. L.; Gagnon, D. R.; Karasz, F. E.; Lenz, R. W. *J. Polym. Sci., Part B: Polym. Phys.* **1986**, *24*, 2793.
(17) Chen, D.; Winokur, M. J.; Masse, M. A.; Karasz, F. E. *Polymer* **1992**, *33*, 3116.
(18) Briers, J.; Eevers, W.; Cos, P.; Geise, H. J.; Mertens, R.; Nagels, P.; Zhang, X. B.; Van Tendeloo, G.; Herrebout, W.; Van der Veken, B. *Polymer* **1994**, *35*, 4569.
(19) Martens, J. H. F.; Marseglia, E. A.; Bradley, D. D. C.; Friend, R. H.; Burn, P. L.; Holmes, A. B. *Synth. Met.* **1993**, *55*−*57*, 449.
(20) Jin, J. I.; Park, C. K.; Shim, H. K. *Polymer* **1994**, 35, 480.
(21) Chen, S. A.; Ni, J. M. *Macromolecules* **1992**, *25*, 6081.
(22) Prosa, T. J.; Winokur, M. J.; Moulton, J.; Smith, P.; Heeger, A. J. *Macromolecules* **1992**, *25*, 4364.
(23) Vahlenkamp, T.; Wegner, G. *Macromol. Chem. Phys.* **1994**, *195*, 1933.
(24) Zheng, W. Y.; Levon, K.; Laakso, J.; Österholm, J. E. *Macromolecules* **1994**, *27*, 7754.
(25) Rodriguez-Parada, J. M.; Duran, R.; Wegner, G. *Macromolecules* **1989**, *22*, 2507.
(26) Ballauff, M. *Makromol. Chem., Rapid Commun.* **1986**, *7*, 407.
(27) Ballauff, M. *Makromol. Chem., Rapid Commun.* **1987**, *8*, 93.
(28) Weder, C.; Wrighton, M. S. *Macromolecules* **1996**, *29*, 5157.
(29) Ofer, D.; Swager, T. M.; Wrighton, M. S. *Chem. Mater.* **1995**, *7*, 418.
(30) Fahlman, M.; Bröms, P.; dos Santos, A. D.; Moratti, S. C.; Johansson, N.; Xing, K.; Friend, R. H.; Holmes, A. B.; Brédas, J. L.; Salaneck, W. R. *J. Chem. Phys.* **1995**, *102*, 8167.
(31) Fahlman, M.; Brédas, J. L. *Synth. Met.* **1996**, *78*, 39.
(32) Neubert, M. E.; Laskos, S. J.; Maurer, L. J.; Carlino, L. T.; Ferrato, J. P. *Mol. Cryst. Liq. Cryst.* **1987**, *44*, 197.
(33) Askari, S. H.; Rughooputh, S. D.; Wudl, F. *Synth. Met.* **1989**, *29*, E129.
(34) Wheland, R. C.; Martin, E. L. *J. Org. Chem.* **1975**, *40*, 3101.
(35) Reinhardt, B. A.; Unroe, M. R. *Polym. Commun.* **1991**, *32*, 85.
(36) Gill, R. E.; van Hutten, P. F.; Meetsma, A.; Hadziioannou, G. *Chem. Mater.* **1996**, *8*, 1341.
(37) Ho, K. S.; Bartus, J.; Levon, K.; Mao, J.; Zheng, W. Y.; Laakso, J.; Taka, T. *Synth. Met.* **1993**, *55*−*57*, 384.
(38) Park, K. C.; Levon, K. *Macromolecules* **1997**, *30*, 3175.
(39) Bolognesi, A.; Porzio, W.; Provasoli, F.; Ezquerra, T. *Makromol. Chem.* **1993**, *194*, 817.
(40) Lee, G. J.; Kim, D.; Lee, J. I.; Shim, H. K.; Kim, Y. W.; Jo, J. C. *Jpn. J. Appl. Phys.* **1996**, *35*, 114.
(41) Faïd, K.; Fréchette, M.; Ranger, M.; Mazerolle, L.; Levesque, I.; Leclerc, M. *Chem. Mater.* **1995**, *7*, 1390.
(42) Chuang, K. R. Ph.D. Thesis, Tsing-Hua University, Hsinchu, Taiwan, 1996.
(43) Graessly, W. W. In *Physical properties of polymers*, 2nd ed.; Mark, J. E., Eds.; American Chemical Society: Washington, DC, 1984.
(44) Chen, S. A.; Lee, S. J. *Synth. Met.* **1995**, *72*, 253.
(45) Qian, R.; Chen, S.; Song, W.; Bi, X. *Macromol. Rapid Commun.* **1994**, *15*, 1.

MA9715076